Development of motor neurons and motor activity in zebrafish requires F-actin nucleation by Fmn2b

Dhriti Nagar[1], Blake Carrington[2], Shawn M Burgess[3] and Aurnab Ghose[1*]

[1] Indian Institute of Science Education and Research (IISER) Pune, Dr Homi Bhabha Road, Pune 411008, INDIA

[2] Zebrafish Core, Translational and Functional Genomics Branch, National Human Genome Research Institute, National Institutes of Health, Bethesda, Maryland, USA

[3] Translational and Functional Genomics Branch, National Human Genome Research Institute (NHGRI), National Institutes of Health (NIH), Bethesda, MD, USA

* Correspondence: Dr. Aurnab Ghose, Indian Institute of Science Education and Research (IISER) Pune, Dr Homi Bhabha Road, Pune 411008, INDIA.

Email: aurnab@iiserpune.ac.in

ABSTRACT

Background

Cytoskeletal remodelling plays a pivotal role in the establishment of neuronal connectivity during development and in plasticity in adults. Mutations in the cytoskeleton regulatory protein Formin-2 (Fmn2) are associated with neurodevelopmental disorders like intellectual disability, though its function in neuronal morphogenesis has not been characterised *in vivo*.

Results

Here we develop a loss-of-function model for *fmn2b*, the zebrafish orthologue of Fmn2, using CRISPR/Cas9-mediated gene editing. *fmn2b* mutants display motor deficits starting from the earliest motor responses in the embryo. We find that *fmn2b* is expressed in spinal motor neurons and its loss reduces motor neuron innervation of the axial muscles without affecting myotome integrity. The translocation of caudal primary (CaP) motor neuron outgrowth is compromised in *fmn2b* mutants, while rostral primary (RoP) motor neurons have missing soma or stall at the horizontal myoseptum. Strikingly, axon collateral branching of the motor neurons is severely compromised and results in reduced synaptic coverage of the myotome. Rescue experiments identify the requirement for Fmn2-mediated actin nucleation for motor neuron outgrowth and arborisation.

Conclusions

The zebrafish loss-of-function model of Fmn2 reveals the specific requirement of F-actin polymerisation by Fmn2 in neuromuscular development. It also underscores the role of Fmn2 in motor neuropathies, especially as a proportion of individuals harbouring mutations in Fmn2 present with hypotonia.

Keywords

Fmn2b, motor behaviour, motor neurons, axonal branching, actin nucleation

INTRODUCTION

Developing neurons migrate to their predetermined targets, undergo axonogenesis, pathfinding and eventually arborize to make functional synapses. Cytoskeletal remodelling allows dynamic interactions of the developing neurons with the environment during outgrowth, pathfinding and arborization (Dickson, 2002; Lowery and Van Vactor, 2009; Gordon-Weeks and Fournier, 2014; Flynn and Bradke, 2020) aided by several actin remodelling proteins (Dent et al., 2011; Kessels et al., 2011; Lewis et al., 2013; Coles and Bradke, 2015; Armijo-Weingart and Gallo, 2017).

Remodelling of actin filaments allows protrusive structures to probe the environment for cues in the form of growth cone filopodia and axonal and dendritic branches (Lowery and Van Vactor, 2009; Lewis et al., 2013; Armijo-Weingart and Gallo, 2017; Menon and Gupton, 2018).

In zebrafish, spinal motor neurons exit perpendicular to the spinal cord and traverse the myotomes to arborize and make synapses onto the axial muscles (Myers et al., 1986; Westerfield et al., 1986). Adequate innervation of muscles by the motor neurons is ensured by hemisegment specific outgrowth, pathfinding and arborization. Precise neuronal morphogenesis of motor neurons is critical for achieving context-specific synaptic drive at the level of muscles, enabling the organism to execute motor behaviours.

Actin nucleating proteins are a major class of actin remodelling factors and have been implicated in neuronal morphogenesis. The actin nucleator Cobl localizes to regions with high actin dynamics and is implicated in the maintenance of neurite branching (Ahuja et al., 2007). Actin nucleators mediate the local rearrangement of actin filaments via the formation of dynamic structures like F-actin patches and F-actin blobs

and regulate the initiation of protrusions and branching (Ketschek and Gallo, 2010; Spillane et al., 2011; Spillane and Gallo, 2014; Nithianandam and Chien, 2018; Kundu et al., 2020). Reports have characterized the role of Dishevelled associated activator of morphogenesis (Daam) formins in *Drosophila* axonal growth (Matusek et al., 2008; Prokop et al., 2011) and Daam1a in habenular morphogenesis and IPN connectivity in zebrafish (Colombo et al., 2013). Another study identified Formin-3 (Form3) in the maintenance of complex dendritic arbours of nociceptive sensory neurons in *Drosophila* via microtubule stabilization and adequate organelle trafficking (Das et al., 2021). However, the function of formin family of actin nucleators in axonal branching *in vivo* remains elusive.

Formin-2 (Fmn2) is part of the FMN family of formins and is known to be involved in neuronal development. Biallelic mutations in Fmn2 cause neurodevelopmental defects resulting in intellectual disability and muscle hypotonia in humans (Law et al., 2014). Primary hippocampal neurons from Fmn2 null mice show defective dendritic spine morphogenesis (Law et al., 2014) and there is increasing evidence implicating copy number variations (CNVs) and single nucleotide polymorphisms (SNPs) in Fmn2 in sporadic Amyotrophic Lateral Sclerosis (SALS) (Schymick et al., 2007; Pamphlett et al., 2011; Morello et al., 2018). Fmn2 has previously been characterized in outgrowth, pathfinding (Sahasrabudhe et al., 2016; Ghate et al., 2020; Kundu et al., 2021) and axonal branching (Kundu et al., 2020) in chick spinal primary neurons *in vitro*. Depletion of Fmn2 causes reduced growth cone motility and mechanotransduction in chick spinal primary neurons (Sahasrabudhe et al., 2016; Ghate et al., 2020). Fmn2 regulates the stabilization of actin patches required for the initiation of axonal branching in cultured chick spinal neurons by insulating the actin patch from actin depolymerizing factors like ADF (Kundu et al., 2020). Morpholino-mediated transient

knockdown of Fmn2b, the zebrafish ortholog of Fmn2, causes impaired outgrowth of the spiral fiber neuron commissures in the hindbrain and results in diminished short latency escape response (Nagar et al., 2021).

In this study, we generate *fmn2b* mutants using the CRISPR-Cas9 based gene editing to assess the contribution of Fmn2b in neural circuit development and behaviour and to improve our understanding of the mechanistic underpinnings of the neurodevelopmental disorders associated with Fmn2.

Motor neurons are the final, executory neurons driving motor responses. In zebrafish, the spinal motor neurons receive synaptic inputs from reticulospinal neurons, including the Mauthner cell and several hindbrain interneurons, which regulate motor neuron function in response to stimuli (Bernhardt et al., 1990; Hale et al., 2001; McLean and Fetcho, 2008). Three subtypes of primary motor neurons are present on either side of the spinal cord – the Caudal primary (CaP), the Middle primary (MiP) and the Rostral primary (RoP) – with distinct morphology and muscle targets (Eisen et al., 1986; Myers et al., 1986; Bernhardt et al., 1990; Melançon et al., 1997; Stifani, 2014). The myotomes are also innervated by secondary motor neurons which develop after the primary motor neurons and have less complex arborization fields (Pike et al., 1992; Beattie et al., 1997; Menelaou and Svoboda, 2009). Motor neurons innervate the target muscles to form structurally and functionally distinct motor units and regulate the overall synaptic drive of the muscles during motor behaviours (Saint-Amant and Drapeau, 1998; Drapeau et al., 2002; Bagnall and McLean, 2014; Bello-Rojas et al., 2019).

116 This study uncovers the role of the zebrafish orthologue of Formin-2, Fmn2b, in
117 regulating spinal motor neuron outgrowth and branching *in vivo* and the consequent
118 effects on motor behaviour.

RESULTS

Generating fmn2b CRISPR mutants

Zebrafish has two paralogs of Formin-2, *fmn2a* and *fmn2b*. *fmn2b*, located on chromosome 12, has higher sequence homology with human Fmn2 compared to *fmn2a* and has the characteristic Formin Homology 1 (FH1), Formin Homology 2 (FH2) and Formin Spire Interaction (FSI) domains (Nagar et al., 2021). In contrast, the FH1 domain of *fmn2a* is truncated. As observed in humans, rodents and chicks (Leader and Leder, 2000; Sahasrabudhe et al., 2016), *fmn2b* mRNA is enriched in the zebrafish nervous system whereas *fmn2a* shows no detectable expression in the nervous system of zebrafish (Nagar et al., 2021). In this study, we used the CRISPR-Cas9 technology to generate mutants of *fmn2b*, the functional ortholog of mammalian Fmn2 in zebrafish.

To generate *fmn2b* knockout zebrafish, sgRNAs targeting the exon 1 of *fmn2b* were designed using the CRISPRscan tool (Moreno-Mateos et al., 2015) and cross verified for high scores using the ZebrafishGenomics track (LaFave et al., 2014) in UCSC genome browser. Exon 1 was targeted to ensure that the resulting mutant would lack the functional domains.

The embryos injected with sgRNA and Cas9 mRNA were raised till sexual maturity. Individual embryos from the injected clutch were outcrossed with wildtype fish of the opposite sex to obtain eggs that were genotyped using fluorescent PCR (Varshney et al., 2016). Multiple founder lines with different allelic mutations were identified for *fmn2b* by fluorescent-PCR. The F1 progeny obtained from the outcross of these founder lines was raised to adulthood and the siblings were in-crossed. The F2 progeny were raised to adulthood and genotyped using the caudal fin clip method and

143 subsequent Sanger sequencing of the genomic locus flanking the sgRNA-1 target
144 sequence to determine whether they were heterozygous or homozygous for the
145 inherited mutant allele.

146 The sgRNA caused various indels near the intended target around 696 bp into the
147 *fmn2b* cDNA sequence in exon 1, corresponding to 232nd amino acid position in the
148 1454 amino acid long Fmn2b protein sequence. Two alleles causing a 4 bp and a 7
149 bp deletion, respectively, were selected to obtain homozygous mutants *fmn2b*$^{\Delta4/\Delta4}$ and
150 *fmn2b*$^{\Delta7/\Delta7}$ (Figure 1 A-B). The 4 bp deletion in the *fmn2b*$^{\Delta4/\Delta4}$ mutant leads to
151 frameshift variant (p.Leu233TrpfsTer281) with Tryptophan as the first amino acid
152 changed in place of Leucine at 233rd amino acid position causing premature stop
153 codon at the 281st amino acid. The 7 bp deletion acid in the *fmn2b*$^{\Delta7/\Delta7}$ results in the
154 frameshift variation (p.Val234ThrfsTer280) with Threonine replacing Valine as the
155 234th amino acid and causing a premature stop codon at 280th amino acid position
156 (Figure 1 C). The two homozygous mutant alleles were in-crossed to obtain
157 heteroallelic *fmn2b* mutants (*fmn2b*$^{\Delta4/\Delta7}$) and used in subsequent experiments.

158 ***fmn2b mutants exhibit Spontaneous Tail Coiling (STC) and Touch-Evoked***
159 ***Escape Response (TEER) deficits***

160 The first motor behaviour to appear in the developing zebrafish embryo is spontaneous
161 tail coiling (STC) which starts around 17 hpf and persists till 27 hpf (Saint-Amant and
162 Drapeau, 1998; Brustein et al., 2003). We recorded the spontaneous tail coiling in
163 *fmn2b*$^{+/+}$ and *fmn2b*$^{\Delta4/\Delta7}$ embryos at 22 hpf (Movie 1). The frequency of spontaneous
164 tail coiling was reduced in *fmn2b*$^{\Delta4/\Delta7}$ mutant embryos (3.168 ± 0.314 min^{-1}) as
165 compared to the wild-type *fmn2b*$^{+/+}$ embryos (5.003 ± 0.203 min^{-1}) (Figure 2 A).
166 However, the maximum amplitude of tail coiling did not change significantly in the
167 *fmn2b*$^{\Delta4/\Delta7}$ embryos (Figure 2 B). The decrease of coiling frequency but not the

magnitude of coiling indicates that the defects are likely due to deficits in the motor neuron or the neuromuscular junction (NMJ) function rather than loss of muscle integrity.

As the embryo develops, the motor circuits mature to mediate touch-evoked escape responses (TEER) beginning at 48 hpf. TEER is typically manifested as a fast C-bend escape followed by a swimming bout. We performed the TEER assay on *fmn2b*$^{+/+}$ and *fmn2b*$^{\Delta 4/\Delta 7}$ embryos at 60 hpf (Movie 2) and recorded their response at 200 fps. Both the distance traversed (13.55 ± 1.06 mm) and the average speed (34.26 ± 2.785 mm/s) of touch-evoked swimming was reduced in 60 hpf *fmn2b*$^{\Delta 4/\Delta 7}$ embryos as compared to the distance covered (65.31 ± 4.93 mm) and swim speed (84.37 ± 3.253) of *fmn2b*$^{+/+}$ embryos (Figure 2 C, D, E). However, the maximum instantaneous speed attained during the entire swim bout was not significantly different between *fmn2b*$^{+/+}$ (199.5 ± 7.039 mm/s) and *fmn2b*$^{\Delta 4/\Delta 7}$ embryos (183.2 ± 6.245 mm/s) (Figure 2 F).

The comparable maximum tail coiling amplitudes and maximum instantaneous speeds observed in *fmn2b*$^{+/+}$ and *fmn2b*$^{\Delta 4/\Delta 7}$ embryos suggest abnormal motor neuron development or NMJ function and is unlikely to involve deficits in the musculature. Consistent with this, phalloidin staining of the *fmn2b*$^{\Delta 4/\Delta 7}$ embryos revealed no structural deformities in the axial muscles compared to the *fmn2b*$^{+/+}$ embryos (Figure S1).

fmn2b mRNA is expressed in the spinal cord and spinal motor neurons of zebrafish embryos

The time window of STC and TEER in zebrafish embryos coincides with the outgrowth and pathfinding of primary motor neurons (Myers et al., 1986). *fmn2b* mRNA was found to be expressed in the spinal cord 48 hpf onwards suggesting a possible role in

192 the development of spinal neurons (Figure 3 A, B). Previous reports have also reported
193 Fmn2 mRNA expression in the spinal cord of chick, mouse and human embryos
194 (Leader and Leder, 2000; Sahasrabudhe et al., 2016). To explicitly test the expression
195 of *fmn2b* mRNA in the motor neurons, GFP positive motor neurons were isolated using
196 Fluorescence-activated cell sorting (FACS) from 24 hpf and 60 hpf *Tg(mnx1:GFP)*
197 embryos and the expression of *fmn2b* evaluated by RT-PCR. *fmn2b* transcript was
198 expressed in motor neurons expressing GFP driven by the Tg(mnx1:GFP) isolated
199 from both 24 hpf and 60 hpf embryos (Figure 3 C). Therefore, *fmn2b* is expressed in
200 the spinal cord and in the spinal motor neurons of zebrafish embryos and could
201 mediate motor neuron development and function.

202 ***CaP motor neuron outgrowth is slower in fmn2b mutants***

203 To test the hypothesis that the motor defects in *fmn2b* mutants may arise due to
204 deficits in motor neuron morphogenesis, the *fmn2b*$^{\Delta 4/\Delta 7}$ mutant line was crossed with
205 the *Tg(mnx1:GFP)* line to obtain homozygous *fmn2b* mutants in the transgenic
206 background of GFP-labelled motor neurons. The development of motor neurons was
207 observed from 22 hpf to 26 hpf using time-lapse confocal imaging of the GFP-labelled
208 neurons (Movie 3). The growth cones of the pioneering caudal primary (CaP) motor
209 neurons were tracked using the Manual Tracking plugin in ImageJ, and the average
210 translocation speed was calculated. The *fmn2b*$^{\Delta 4/\Delta 7}$ embryos showed slow outgrowth
211 of the CaP neurons (Figure 3 D, E). The growth cone translocation speed of *fmn2b*$^{\Delta 4/\Delta 7}$
212 embryos (22.1 ± 1.575 µm/h) was slower than the *fmn2b*$^{+/+}$ embryos (28.34 ± 1.962
213 µm/h) (Figure 3 F).

214 ***Primary motor neuron outgrowth and branching defects in fmn2b mutants***

In addition to the slow outgrowth of CaP motor neurons in *fmn2b* mutants, collateral branches extended by the motor neurons at 24 hpf (Figure 4 A, B) and 60 hpf (Figure 4 G, H) were observed using the *fmn2b* mutant line *fmn2b*$^{\Delta4/\Delta7}$ in the background of the transgenic line *Tg(mnx1:GFP).* The embryos were mounted laterally to image the motor neurons and the images traced and quantified using the NeuronJ plugin in ImageJ. At 24 hpf, 100% of the hemisegments had the CaP motor neuron soma present in *fmn2b*$^{+/+}$ as well *fmn2b*$^{\Delta4/\Delta7}$ embryos. The branch density along the fascicle length (Figure 4 E) and the length of the motor fascicle (Figure 4 F) extended by the primary motor neurons at 24 hpf was found to be reduced in *fmn2b*$^{\Delta4/\Delta7}$ embryos. Similarly, 60 hpf *fmn2b*$^{\Delta4/\Delta7}$ embryos showed a reduction in the density (Figure 4 K) of collateral branches along the motor fascicle along with a reduction in the fascicle length (Figure 4 L). Similar defects were observed in homozygous *fmn2b* mutants with the *fmn2b*$^{\Delta4}$ and *fmn2b*$^{\Delta7}$ alleles (Figure S3).

These observations implicate *fmn2b* function in both the outgrowth of the CaP motor neuron and collateral branching of motor neurons.

F-actin nucleation activity of Fmn2 is required for motor neuron branching

The functional domains characteristic of Formin-2 are conserved across vertebrates and ectopic expression of full-length mouse Fmn2 (mFmn2) can rescue neurodevelopmental defects induced by morpholino-mediated knockdown of Fmn2b in zebrafish (Nagar et al., 2021). To assess if the expression of exogenous Fmn2 could rescue the outgrowth and branching defects, *mFmn2* mRNA tagged with mCherry was injected in the *fmn2b*$^{\Delta4/\Delta7}$ mutant embryos at the 1-cell stage. The branch density and fascicle length defects were rescued in both 24 hpf (Figure 4 C, E, F) and 60 hpf (Figure 4 I, K, L) mutant embryos.

F-actin nucleation is the canonical function of formins, including Fmn2, and is mediated by the FH2 domain (Goode and Eck, 2007; Quinlan et al., 2007; Yoo et al., 2015). The FH2 domain is conserved across phyla, including zebrafish (Nagar et al., 2021). A conserved isoleucine residue (at position 1226 in mouse Fmn2) is known to be critical for actin nucleation (Quinlan et al., 2007; Roth-Johnson et al., 2014; Kundu et al., 2020). Clustal omega alignment of the conserved isoleucine residue is shown in Figure S2. To test if actin nucleation by Fmn2b is required in zebrafish motor neuron morphogenesis, an F-actin nucleation dead version of mFmn2 with a point mutation converting the Isoleucine at 1226 amino acid position to Alanine (mFmn2-I1226A) was used. The mRNA for mFmn2-I1226A tagged with mCherry was injected in the *fmn2b*$^{\Delta 4/\Delta 7}$ embryos at the 1-cell stage and the motor neuron development was analyzed.

The *mFmn2-I1226A* mRNA injected 24 hpf (Figure 4 D, E, F) and 60 hpf (Figure 4 J, K, L) mutant embryos continue to exhibit the outgrowth and branching defects similar to the *fmn2b*$^{\Delta 4/\Delta 7}$ embryos. Rescue of phenotype exhibited by the *fmn2b*$^{\Delta 4/\Delta 7}$ mutants by full-length mFmn2 but not the nucleation dead version, mFmn2-I1226A points towards the conserved function of Fmn2 in motor neuron development and highlights the significance of F-actin nucleation by Fmn2 in outgrowth and branching of motor neurons.

Rostral Primary (RoP) motor neuron development is compromised in fmn2b mutants

Despite slower outgrowth rates and reduced branching in *fmn2b*$^{\Delta 4/\Delta 7}$ embryos, the CaP fascicle eventually reaches the extremity of the ventral musculature in the zebrafish flank. On the contrary, another class of primary motor neurons, the Rostral primary (RoP) motor neurons which typically project to the mid-dorsal and mid-ventral

musculature (Bagnall and McLean, 2014; Bello-Rojas et al., 2019), are permanently affected in *fmn2b*$^{\Delta4/\Delta7}$ embryos. The RoP soma are located at their predetermined site adjacent to the CaP and VaP cell body cluster in the spinal cord. The cell bodies of primary motor neurons are distinctly recognizable at 24 hpf.

On examining the 24 hpf embryos, the RoP cell body was found to be missing in *fmn2b* mutants. Compared to 2.5% of the hemisegments in *fmn2b*$^{+/+}$ embryos, 46.87% of the hemisegments in *fmn2b*$^{\Delta4/\Delta7}$ embryos did not have the RoP cell body. Injection of 1-cell stage *fmn2b*$^{\Delta4/\Delta7}$ embryos with *mFmn2* mRNA rescued this defect with only 2.85% hemisegments lacking RoP soma. However, the actin nucleation dead *mFmn2-I1226A* mRNA failed to rescue the loss of RoP soma in *fmn2b* mutants and 43.75% of the hemisegments continued to show loss of RoP soma (Figure 5 A-F).

At 60 hpf, the RoP motor neurons innervate their target in the mid-dorsal and mid-ventral musculature. The RoP motor neurons in *fmn2b*$^{\Delta4/\Delta7}$ mutants showed two major types of defects, absence of RoP outgrowth and stalling of RoP at the choice point near the horizontal myoseptum (HMS), where the RoP axons take a sharp lateral turn.

In the *fmn2b* mutant embryos, 91.3% of the hemisegments analyzed showed little to no lateral innervation. Of these, 44.35% of the hemisegments displayed defasciculated axons near the horizontal myoseptum, which acts as a choice point for the RoP axons to turn laterally. The hemisegments with defasciculated axons were classified as stalled RoP axons. Similar defects in RoP-like secondary motor neurons have been reported to occur due to depletion of Kif1b and Fidgetin like-1 in zebrafish (Fassier et al., 2018; Atkins et al., 2019). However, 46.95% of hemisegments had no RoP innervation altogether and were classified as RoP absent. Only 8.7% hemisegments showed the stereotypical RoP innervation and were classified as RoP present. In the *fmn2b*$^{+/+}$ embryos, only 3.15% of the hemisegments quantified showed RoP stalling

289 defects, and the rest had stereotypical innervation by the RoP neurons. The RoP
290 stalling and outgrowth defects were rescued by injection of full-length *mFmn2* mRNA
291 with only 10.16% hemisegments with RoP stalling and 8.47% hemisegments with RoP
292 outgrowth defects. On the other hand, RoP defects persisted in the *fmn2b*$^{\Delta 4/\Delta 7}$
293 embryos injected with *mFmn2-I1226A* mRNA, with 18.3% of hemisegments having
294 stalled RoP axons and 81.7% without RoP innervation (Figure 5 G-L).

295 Collectively, these results indicate that *fmn2b* has pleiotropic effects on RoP
296 development dependent on F-actin nucleation function. The deficits are at the level of
297 loss of RoP soma, deficits in RoP axonogenesis and stalling at the horizontal
298 myoseptum choice point.

299 ***Overexpression of Fmn2 but not the nucleation dead mutant increases collateral***
300 ***branching in motor neurons***

301 The role of *fmn2b* in motor neuron development has been established so far by
302 observing *fmn2b* mutants, where the loss of Fmn2b in motor neurons causes a
303 reduction in outgrowth and branching. Overexpression of mouse Fmn2 was employed
304 in wildtype embryos to test the phenotypes in the context of Fmn2 gain of function.
305 The embryos overexpressing mFmn2 showed increased branching, but
306 overexpression of the nucleation dead mFmn2-I1226A did not cause any significant
307 changes and was comparable to the wild-type embryos (Figure 6 A, B, E, F). The
308 branch density was found to be increased in mFmn2 mRNA injected embryos at 24
309 hpf as well as 60 hpf but not in mFmn2-I1226A mRNA injected group (Figure 6 C, G).
310 Interestingly, in 24 hpf embryos, the fascicle length was not significantly different in
311 embryos overexpressing mFmn2 but was found to be decreased in embryos
312 overexpressing mFmn2-I1226A. In 60 hpf embryos, the fascicle length was slightly

313 increased in the mFmn2 overexpression group but remain unaffected in the mFmn2-
314 I1226A overexpression group (Figure 6 D, H).

315 However, quantification of RoP soma and RoP axon outgrowth phenotypes in the
316 *fmn2b*$^{+/+}$ embryos overexpressing mFmn2 and mFmn2-I1226A did not reveal any
317 significant changes (Figure S4).

318 ***Neuromuscular Junction (NMJ) development in fmn2b mutants***

319 Primary motor neurons innervate the fast-twitch muscles and form functional synapses
320 by 48 hpf. To visualize the neuromuscular junctions (NMJ), double immunostaining of
321 whole-mount 60 hpf embryos with znp-1 antibody (presynaptic marker) and α-
322 bungarotoxin (post-synaptic marker) were undertaken. The co-localization of the pre-
323 and post-synaptic markers revealed the engaged NMJ synapses in *fmn2b*$^{+/+}$ and
324 *fmn2b*$^{\Delta 4/\Delta 7}$ embryos (Figure 7 A, B). Synapses (co-localization of znp-1 and α-
325 bungarotoxin signals) along the neuronal arbours were quantified using the
326 SynapCountJ plugin in Fiji. The number of synapses identified was normalized to the
327 area of the myotome corresponding to one somite and the length of the neuronal
328 arbour.

329 The *fmn2b*$^{\Delta 4/\Delta 7}$ mutants show reduced synaptic coverage of the myotomes compared
330 to *fmn2b*$^{+/+}$ embryos (Figure 7 C). This result is consistent with previous observations
331 of reduced outgrowth and branching density, and therefore the attenuated occupancy
332 of myotome area, of motor neurons.

333 However, the number of synapses normalized to the arbour length was found to be
334 comparable (Figure 7 D). Thus, while the ability of motor neurons to form synapses is
335 intact in *fmn2b* mutants, the dramatically reduced arborization results in an effective
336 reduction in the total number of synapses per myotome. The locomotor defects

337 observed in *fmn2b* mutants is consistent with the decrease in the total number of

338 synapses per myotome leading to insufficient activation of the myotome.

DISCUSSION

Mutations, including loss-of-function mutations, in Fmn2 have been associated with intellectual disability, sensory dysfunction, age-associated cognitive decline (Perrone et al., 2012; Law et al., 2014; Agís-Balboa et al., 2017; Marco et al., 2018; Gorukmez et al., 2020). Interestingly, some affected individuals also develop hypotonia (Law et al). Further, mutations in Fmn2 have also been associated with sporadic amyotrophic lateral sclerosis in multiple studies (Schymick et al., 2007; Pamphlett et al., 2011; Morello et al., 2018). These associations suggest a possible involvement of Fmn2 in motor neuron development and function.

In this study, we generated *fmn2b* mutants using the CRISPR-Cas9 system (Figure 1) and found locomotor deficits in the homozygous mutants. *The fmn2b* mutants displayed deficits right from the earliest motor behaviours (STC at 22 hpf; Figure 2) to later stages where the development of the embryonic neural circuits is complete (TEER at 60 hpf; Figure 2). *fmn2b* mRNA expression was also detected in motor neurons and the spinal cord (Figure 3). Systematic evaluation of the primary spinal motor neurons revealed defects in the outgrowth of the CaP motor neurons. Live imaging indicated that the growth cone translocation velocity was reduced in *fmn2b*$^{\Delta 4/\Delta 7}$ embryos (Figure 3).

Recent *in vitro* studies in chick spinal neurons implicates Fmn2 in growth cone translocation. These studies implicate Fmn2 in mediating a molecular clutch that stabilizes the contact sites between the growth cone and the extracellular matrix and regulates the generation of traction forces required for outgrowth (Sahasrabudhe et al., 2016; Ghate et al., 2020). Additionally, Fmn2 facilitates the stabilization of protrusive processes, like growth cone filopodia, by coupling exploratory microtubules

363 with the F-actin cytoskeleton (Kundu et al., 2021). Consistent with this, the depletion
364 of Fmn2 reveals altered microtubule dynamics in the growth cones of zebrafish Rohon-
365 Beard neurons *in vivo*. Similar mechanisms involving actin and microtubule
366 remodelling could be involved in the translocation of CaP growth cones in zebrafish.

367 Even more striking than the delayed outgrowth rates of CaP motor neurons, the
368 development of collateral branches which provide synaptic coverage of the entire
369 muscle field was severely affected (Figure 4). The staggered development of spinal
370 motor neurons in two phases allowed us to selectively look at the innervation of
371 muscles by primary motor neurons at 24 hpf and collectively look at primary and
372 secondary motor neuron innervation at 60 hpf. In addition, the 60 hpf embryos have
373 elaborate branching and fully functional NMJ synapses allowing characterization of
374 *fmn2b* in outgrowth, branching and synapse formation in motor neurons.

375 In 24 hpf *fmn2b* mutant embryos, branch density along the fascicle extended by the
376 primary motor neurons and the fascicle length itself was reduced, suggesting a
377 decrease in the innervation of the target fast muscle fibers (Figure 4). Similarly, the 60
378 hpf *fmn2b*$^{\Delta 4/\Delta 7}$ embryos have reduced branch density and fascicle outgrowth
379 compared to wild-type embryos and are likely to result in reduced speed and distance
380 covered by *fmn2b* mutants (Figure 4). Deficits in motor neuron outgrowth and collateral
381 branching at both 24 hpf and 60 hpf was rescued by overexpressing mouse full length
382 Fmn2 in the *fmn2b* homozygous mutants (Figure 4).

383 Axon collateral branching is a finely regulated multi-step process initiated by the rapid
384 assembly of F-actin resulting in a filopodia-like protrusion from the axonal shaft
385 (Ketschek and Gallo, 2010; Gallo, 2011, 2016; Coles and Bradke, 2015; Ketschek et
386 al., 2015; Armijo-Weingart and Gallo, 2017; Menon and Gupton, 2018). Further
387 cytoskeleton remodelling involving both the actin and microtubule cytoskeletons

388 stabilize the protrusion and extend it to a collateral branch (Gallo, 2011, 2016; Armijo-
389 Weingart and Gallo, 2017). The formation of the lateral protrusion from the axonal
390 shaft is a major rate-limiting step in collateral branching and is initiated by the
391 development of a juxtamembrane F-actin patch. *In vitro* studies implicate several actin
392 binding proteins in regulating axonal F-actin patches. These include the actin
393 nucleating Arp2/3 complex, Drebrin, WVE-1/WAVE regulatory complex (WRC) and
394 cortactin (Spillane et al., 2011; Hu et al., 2012; Chia et al., 2014; Spillane and Gallo,
395 2014; Ketschek et al., 2016; Balasanyan et al., 2017). Recently, Fmn2 has been
396 implicated in collateral branch formation in chick spinal neurons *in vitro*. Fmn2 appears
397 to regulate the lifetime of axonal F-actin patches and consequently the probability of
398 branch initiation (Kundu et al., 2020).

399 The F-actin nucleation and elongation activity of Fmn2 has been characterized *in vitro*
400 (Montaville et al., 2014, 2016). Abrogation of F-actin nucleation activity of Fmn2 can
401 be achieved by mutating a conserved Isoleucine residue in the FH2 domain to Alanine
402 (Quinlan et al., 2007; Roth-Johnson et al., 2014; Kundu et al., 2020). We employed
403 the full-length mouse Fmn2 bearing the isoleucine to alanine mutation (mFmn2-
404 I1226A) in rescue experiments to test if the F-actin nucleating/elongating activity is
405 necessary for motor neuron development.

406 Expression of mFmn2-I1226A in the *fmn2b* mutants could not rescue the outgrowth
407 and branching defects of the motor neurons in 24 hpf and 60 hpf embryos (Figure 4).
408 The failure of mFmn2-I1226A in rescuing the defects underscores the significance of
409 the actin nucleating activity of Fmn2b in motor neuron outgrowth and branching
410 consistent with reports from primary neuronal cultures of chick spinal cord reported
411 previously (Kundu et al., 2020). Therefore, the motor neuron development in zebrafish
412 is dependent on the F-actin nucleation activity of Fmn2b.

Loss of fmn2b had pleiotropic effects on the development of the RoP motor neuron. The RoP soma and RoP outgrowth were severely affected in *fmn2b* mutants. At 24 hpf, multiple hemisegments in *fmn2b* mutants did not have RoP soma at its characteristic position in the spinal cord (Figure 5). The role of Fmn2 in the regulation of differentiation or specification of progenitors is not formally tested despite several studies indirectly indicating pathways involving Fmn2 in cell differentiation. In a recent report, Fmn2 has been shown to cause neural progenitor differentiation defects Fmn2 and Flna double knockout mice in a synergistic manner (Lian et al., 2016). The absence of RoP soma in zebrafish *fmn2b* mutants may indicate a possible role of *fmn2b* in neural progenitor specification and/or differentiation. The RoP soma was seen in the expected location in *fmn2b*$^{\Delta 4/\Delta 7}$ embryos injected with mFmn2 mRNA but the defect could not be rescued by the injection of mFmn2-I1226A mRNA. Interestingly, the F-actin nucleating activity of Fmn2 is required for the differentiation of motor neuron progenitors or their specification. These results open up new possibilities to uncover the mechanistic role of Fmn2 in neural development.

In wild-type zebrafish embryos, the lateral projections from RoP motor neurons and follower secondary motor neurons begin outgrowth later than CaP and MiP neurons (Kuwada, 1993; Liu et al., 2016). In 60 hpf *fmn2b* mutants, the side branches of RoP motor neurons innervating the horizontal myoseptum were either not detected (46% embryos) or appeared to be stalled at the choice point (44% embryos), i.e., the horizontal myoseptum (Figure 5). RoP-like secondary motor neurons, which follow the same trajectory as RoP primary motor neurons have previously been shown to have pathfinding and stalling defects at the horizontal myoseptum in Fidgetin like-1 and Kif1b mutants (Fassier et al., 2018; Atkins et al., 2019). Similarly, the stalled RoP axons appear defasciculated in 60 hpf *fmn2b* mutants

One of the factors contributing to RoP outgrowth defects leading to the absence of RoP innervation in *fmn2b* mutants could be the lack of RoP soma as seen in 24 hpf mutant embryos. Further, the RoP stalling defect implicates Fmn2b in axonal pathfinding in response to guidance cues at the choice point. RoP outgrowth and stalling together caused a noticeable reduction in the innervation of the mid-dorsal and mid-ventral region of the axial myotome. The RoP may be more severely affected than the CaP neurons due to their late axonogenesis concomitant with the pleiotropic function and late expression of *fmn2b* in the spinal cord at 48 hpf.

Intriguingly, the overexpression of mouse Fmn2 in *fmn2b*$^{+/+}$ (wild-type) embryos causes opposite effects as compared to *fmn2b* knockout manifested as hyperbranching. This implies a significant role for *fmn2b* in regulating the collateral branching of motor neurons. Further, overexpression of the nucleation dead version of mFmn2 does not result in increased branch density and underscores the involvement of actin nucleation activity of Fmn2 (Figure 6).

Analysis of NMJ synapses using znp-1 and α-bungarotoxin double staining in *fmn2b* mutants showed no changes in the number of synapses along the total length of the motor neuron branches but showed a reduction in the total number of synapses when normalized to the area of the target myotome. We suggest that the Fmn2b has a primary role in regulating motor neuron branching and not in the formation of NMJ synapses. The behavioural defects in *fmn2b* mutants are likely due to the muscles not receiving sufficient input due to inadequate branching (Figure 7).

In a recent study, prolonged exposure of zebrafish larvae to strong and variable water currents caused upregulation of Fmn2b (Langebeck-Jensen et al., 2019). The rapid upregulation of Fmn2b in response to environmental stressors involving swimming and force generation in larvae with pre-established motor neural circuits invoke the

possible involvement of *fmn2b* in neuronal plasticity and requires systematic investigation.

Taken together, the zebrafish model of Fmn2 loss-of-function offers unexpected insight into spinal motor neuron development and innervation of axial muscles. In addition to identifying the requirement of actin polymerization by Fmn2 in motor neuron morphogenesis and motor outputs, it highlights the central role of cytoskeleton remodelling in motor neuron homeostasis and the development of neuropathies.

METHODS

Zebrafish maintenance and procedures

All protocols used in this study were approved by the Institutional Animal Ethics Committee and the Institutional Biosafety Committee of IISER Pune or a National Human Genome Research Institute (NHGRI/NIH) Animal Care and Use Committee approved animal study protocol. The TAB5 wildtype strain of zebrafish was used for all the experiments including generation of CRISPR mutants. The TAB5 strain was used for all the wildtype outcrosses. Breeding pairs of adult zebrafish were maintained in recirculating aquaria (Techniplast) under a 14h-10h light-dark cycle. The temperature was maintained at 28.5˚C and the pH was buffered between 7.2 to 7.8. The breeding adults were crossed to obtain embryos which were collected and grown in E3 buffer and used at different stages of development as indicated (Kimmel et al., 1995). For immunostaining and live imaging experiments, the buffer was supplemented with 0.003% Phenylthiourea (PTU; Sigma) to remove pigmentation from the skin. The transgenic line *Tg(mnx1:GFP)* was used to visualize motor neurons wherein the *mnx1* promoter specific to motor neurons drives GFP expression (Flanagan-Steet et al., 2005).

Whole mount in situ hybridization

The RNA probes and procedure used for whole mount *in situ* hybridization experiments have been described previously (Nagar et al., 2021).

Isolation of motor neurons from transgenic embryos, FACS, RT-PCR

Single cell suspension was made from around 200 *Tg(mnx1:GFP)* embryos as previously described (Bresciani et al., 2018). Briefly, the embryos were dissociated by trypsinization and filtering through a 70 µm sieve to obtain single cell suspension in

494 1X DMEM containing 10% FBS. The cells were sorted using a BD Biosciences
495 fluorescence-activated cell sorting (FACS) equipment selecting cells expressing GFP,
496 i.e., the motor neurons. RNA was extracted using Qiagen RNeasy Kit and cDNA was
497 prepared using the SuperScript IV RT Kit (ThermoFisher). The cDNA was used for
498 amplifying *fmn2b* transcripts in the mnx1 positive motor neurons. Primers and PCR
499 protocol used to test the presence of *fmn2b* transcripts in motor neurons tagged by
500 *Tg(mnx1:GFP)* were the same as the ones used for amplification of ISH probes from
501 cDNA.

502 **RNA injections**

503 Capped mRNA was synthesized using the HiScribe™ T7 ARCA mRNA Kit (with
504 tailing) from linearized DNA template containing T7 promoter sequence upstream of
505 the mFmn2-mCherry and mFmn2-I1226A-mCherry constructs. The transcribed mRNA
506 was purified using RNeasy MinElute Cleanup Kit (Qiagen). 150 pg of mFmn2-mCherry
507 and mFmn2-I1226A-mCherry mRNA was injected in the zebrafish embryos of desired
508 genotype at 1-cell stage.

509 **sgRNA and Cas9 injections for CRISPR mutants**

510 sgRNA targeting exon 1 of *fmn2b* was designed as previously described (Varshney et
511 al., 2016). T7 HiScribe kit (NEB) was used to transcribe the sgRNA DNA template with
512 the appended T7 promoter. The sgRNA was purified using ZymoResearch clean up
513 columns. T3 mMessage mMachine RNA synthesis kit (Ambion) was used to
514 synthesize capped Cas9 mRNA from the pT3TS-nCas9n plasmid (kind gift from Dr
515 Wenbiao Chen; Addgene plasmid # 46757). The synthesized Cas9 mRNA was
516 purified using the RNeasy MinElute Cleanup Kit (Qiagen). 30 pg sgRNA and 300 pg

517 Cas9 mRNA was injected in zebrafish embryos at 1 cell stage. The sequence of
518 sgRNA is given below.

519 Fmn2b_sgRNA : GGGCGAGAGGCCTCGGCTGG

520 (ENSDARG00000061778.6; 12:47451436-47451459, plus strand)

521 **Genotyping CRISPR mutants**

522 For identifying founder lines for *fmn2b* mutants, fluorescent PCR was performed and
523 analyzed by capillary gel electrophoresis using the ABI GeneAnalyzer 3730XL, as
524 previously described (Carrington et al., 2015; Varshney et al., 2015, 2016).
525 Identification of homozygous mutant lines was also done using Sanger sequencing.
526 Two zebrafish mutant lines with alleles causing a premature stop codon due to a
527 frameshift mutation were established. The homozygous mutants were crossed to each
528 other to obtain a heteroallelic mutant line for *fmn2b* to reduce the effect of any
529 background mutations in the two mutant lines due to unintended off-target effects.
530 Primer sequences for sanger sequencing of genomic DNA amplicons from crispants
531 are as follows:

Fmn2b_PCR_F	AAGCGTAAGAACCAGAATAAGC
Fmn2b_PCR_R	TCATCCGAATGGCTTGC

532

533 **Whole mount immunostaining**

534 PTU treated embryos were collected at desired stages and fixed in 4% formaldehyde
535 overnight at 4˚C. For staining actin structures, fixed embryos were washed with 0.5%
536 PBS-Triton, permeabilized with 2% PBS-Triton for 2 hours at room temperature and

then incubated in Phalloidin Alexa Fluor 568 diluted 1:50 in 2% PBS Triton overnight at 4 °C in dark.

Neuromuscular junction labelling and quantification

For neuromuscular junction staining of embryos, znp-1 antibody (DSHB; 1:100) and Tetramethyl Rhodamine labelled α-bungarotoxin (Invitrogen; 1:200) were used as pre-synaptic and post-synaptic markers respectively. Whole mount immunostaining procedures described in previous section were followed as described. The synapses were counted using the SynapCountJ plugin after making the traces of arbours in NeuronJ plugin in Fiji.

Fluorescence microscopy, live imaging and mounting procedure

All the microscopic imaging was performed on the inverted LSM 780 confocal microscope (Zeiss) with a 25x oil immersion objective (NA 1.4). For imaging of the fixed samples, the embryos were cleared in 50% glycerol and mounted dorsal side down on a glass bottom petri dish using low gelling agarose (Sigma). For live imaging, the live embryos were mounted laterally in 0.5% low melt point agarose (Sigma) containing 0.003% MS-222 (Sigma) in a coverslip bottom 35 mm petri plate.

The growth cone of motor neurons was visualized using the *Tg(mnx1:GFP)* in wildtype or mutant background. The embryos were imaged starting at 22 hpf for 4-6 hours every 3 minutes. The growth cone translocation was analyzed using the Manual tracking plugin in Fiji to track the movement of the leading edge across time. The coordinates obtained were analyzed using the ibidi Chemotaxis tool to calculate the average growth cone translocation speed.

Behaviour experiment set up and behaviour analysis

Spontaneous tail coiling (STC) assay

Embryos 22 hpf within their chorions were transferred to a 35 mm petri plate containing E3 buffer at of 28.5˚C. A video camera (AVT Pike, F-032B) was used to record the spontaneous tail coiling behaviour of the embryos for a time period of 3 minutes at 15 fps. The videos were processed and analysed using a MATLAB script ZebraSTM published previously (González-Fraga et al., 2019).

Touch evoked escape response (TEER) assay

60 hpf zebrafish embryos were housed in a 35 mm petri plate containing pre-warmed E3 buffer at 28.5 ˚C. A tuberculin needle was repurposed by attaching a soft nylon fiber in front of the syringe holding the needle, to deliver tactile stimuli to zebrafish embryos. A soft touch was delivered to the head of the zebrafish once and their behaviour was recorded using a high-speed video camera (AVT Pike F-032B) at 208 fps. The videos obtained were analyzed using the Manual tracking plugin in Fiji to mark the trajectories of the zebrafish embryos upon receiving the tactile stimulus. The tracks were further analyzed using the ibidi Chemotaxis tool to calculate the distance travelled and average speed. The maximum instantaneous speed was calculated manually from the coordinates obtained from the manual tracking output.

Figures and Statistical analysis

The analysis was performed for all the experiments in a genotype blinded manner. Image analysis was performed using Fiji and the Figure panels were assembled using Inkscape. The Violin plots were plotted in GraphPad Prism 8 and indicated statistical tests were performed using GraphPad Prism 8. The data is represented as mean ± SEM in the text. The statistical test used and the p values are indicated in the Figure legends.

AVAILABILITY OF DATA AND MATERIALS

The data generated and analyzed in this study are included in this article and the additional information files. More information can be made available upon reasonable request to the corresponding author.

589 # FIGURES

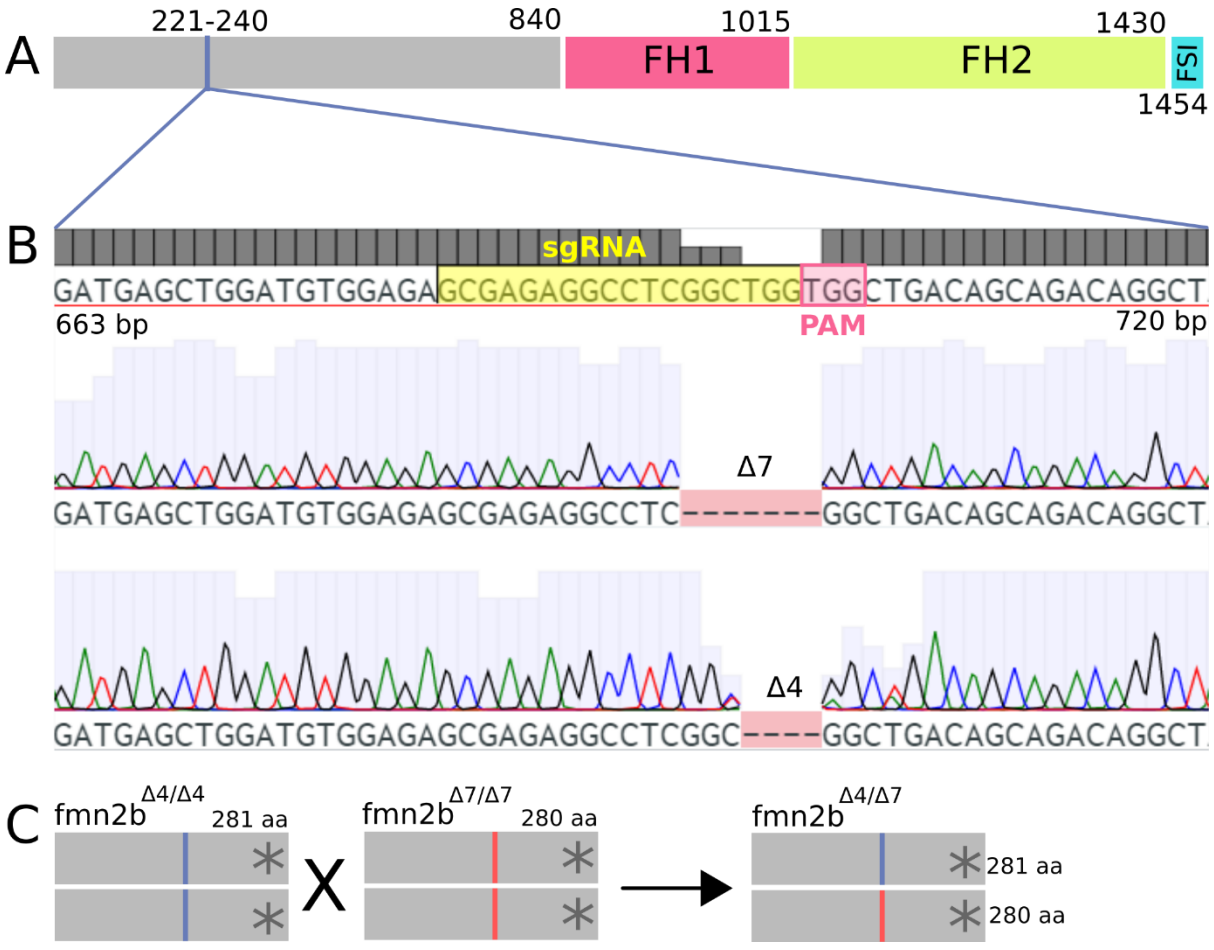

590

591 **Figure 1. Generation of *fmn2b* CRISPR mutants. A)** Schematic of the *fmn2b* protein
592 indicating the functional protein domains and the site of *fmn2b* sgRNA-1. The FH1
593 domain spans the 841-1015 amino acids, FH2 domain spans the 1016-1430 amino
594 acids and the FSI domain spans the 1431-1454 amino acids. **B)** Genomic locus from
595 *fmn2b* exon 1 starting from 663 bp to 720 bp (corresponding to 221-240 amino acids).
596 The sgRNA sequence is highlighted in yellow followed by the PAM sequence in pink.
597 Representative chromatograms of amplicons sequenced from homozygous CRISPR
598 mutants for *fmn2b* show two alleles with a 7 bp and a 4 bp deletion, respectively. The
599 two alleles are denoted as *fmn2b*$^{\Delta 7}$ (p.Leu233TrpfsTer281) and *fmn2b*$^{\Delta 4}$
600 (p.Val234ThrfsTer280). **C)** Schematic outlining the generation of *fmn2b* homozygous

mutants. Fish homozygous for two alleles are denoted as *fmn2b*$^{\Delta 7/\Delta 7}$ and *fmn2b*$^{\Delta 4/\Delta 4}$, the heteroallelic combination is denoted as *fmn2b*$^{\Delta 4/\Delta 7}$.

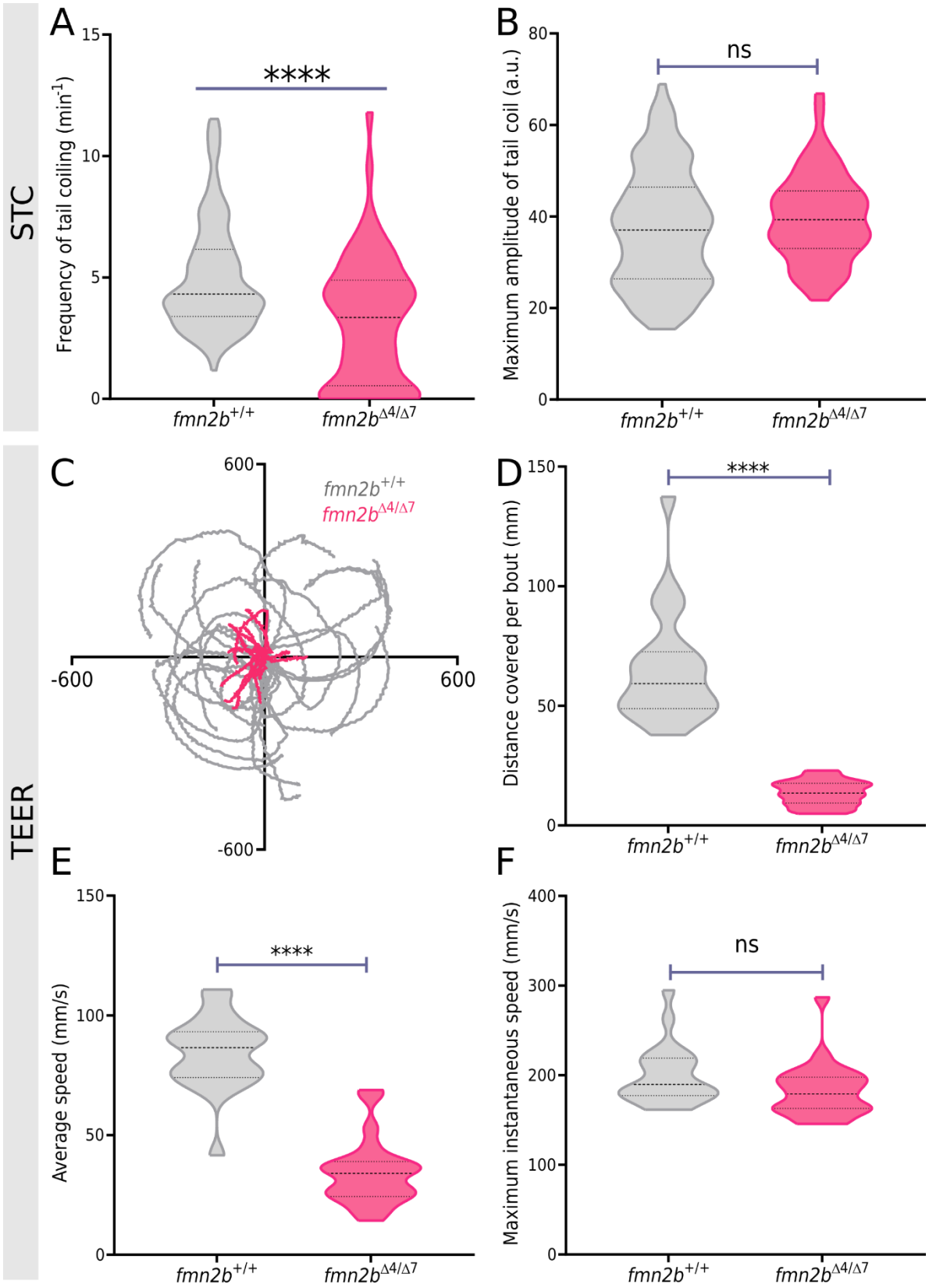

603

604 **Figure 2. *fmn2b* mutants exhibit motor defects. A)** Spontaneous tail coiling (STC)

605 frequency and **B)** maximum amplitude of tail coiling in 22 hpf *fmn2b*$^{+/+}$ (n=121) and

606 *fmn2b*$^{\Delta4/\Delta7}$ (n=68) embryos. **C)** Trajectories of 2 dpf *fmn2b*$^{+/+}$ (grey traces; n=22) and
607 *fmn2b*$^{\Delta4/\Delta7}$ (pink traces; n=24) embryos in Touch Evoked escape response (TEER),
608 re-centered to a common origin for representation. The x and y axes in the plot
609 correspond to the pixel values corresponding to coordinates of the fish from
610 consecutively acquired frames. Quantification of **D)** distance covered per swim bout,
611 **E)** average speed during the swim bout, and **F)** maximum instantaneous swimming
612 speed of 2 dpf *fmn2b*$^{+/+}$ (n=22) and *fmn2b*$^{\Delta4/\Delta7}$ (n=24) embryos in response to a tactile
613 stimulus. (**** p-value <0.0001; ns- not significant; Mann-Whitney U test)

614

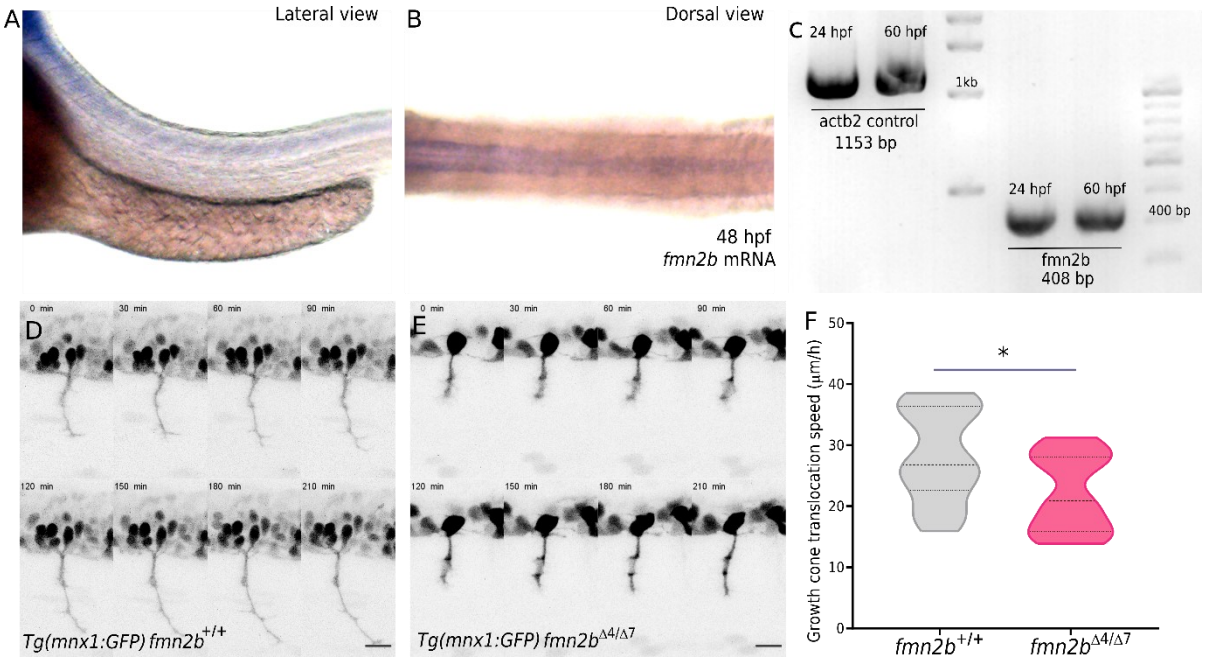

Figure 3. *fmn2b* is expressed in the spinal cord and motor neurons of zebrafish embryos. *fmn2b* is required for motor neuron growth cone translocation

A) Lateral and **B)** dorsal views of a representative 60 hpf embryo showing *fmn2b* mRNA expression in the spinal cord. **C)** Gel showing bands for amplified β2-actin (actb2) control and *fmn2b* from cDNA obtained from FACS sorted motor neurons (mnx1:GFP positive cells) isolated from 24 hpf and 60 hpf wild-type *Tg(mnx1:GFP)* embryos. **D)** Representative montages of live imaging of growth cone translocation in *fmn2b*$^{+/+}$ and **E)** *fmn2b*$^{\Delta4/\Delta7}$ embryos in the background of *Tg(mnx1:GFP)* during the time period of 22 hpf to 26 hpf. **F)** Quantification of motor neuron growth cone translocation speed in *fmn2b*$^{+/+}$ (n=15 growth cones; N=3 embryos) and *fmn2b*$^{\Delta4/\Delta7}$ (n=16 growth cones; N=4 embryos). (* p-value = 0.0298; Mann-Whitney U test). Scale bar is equivalent to 20 µm.

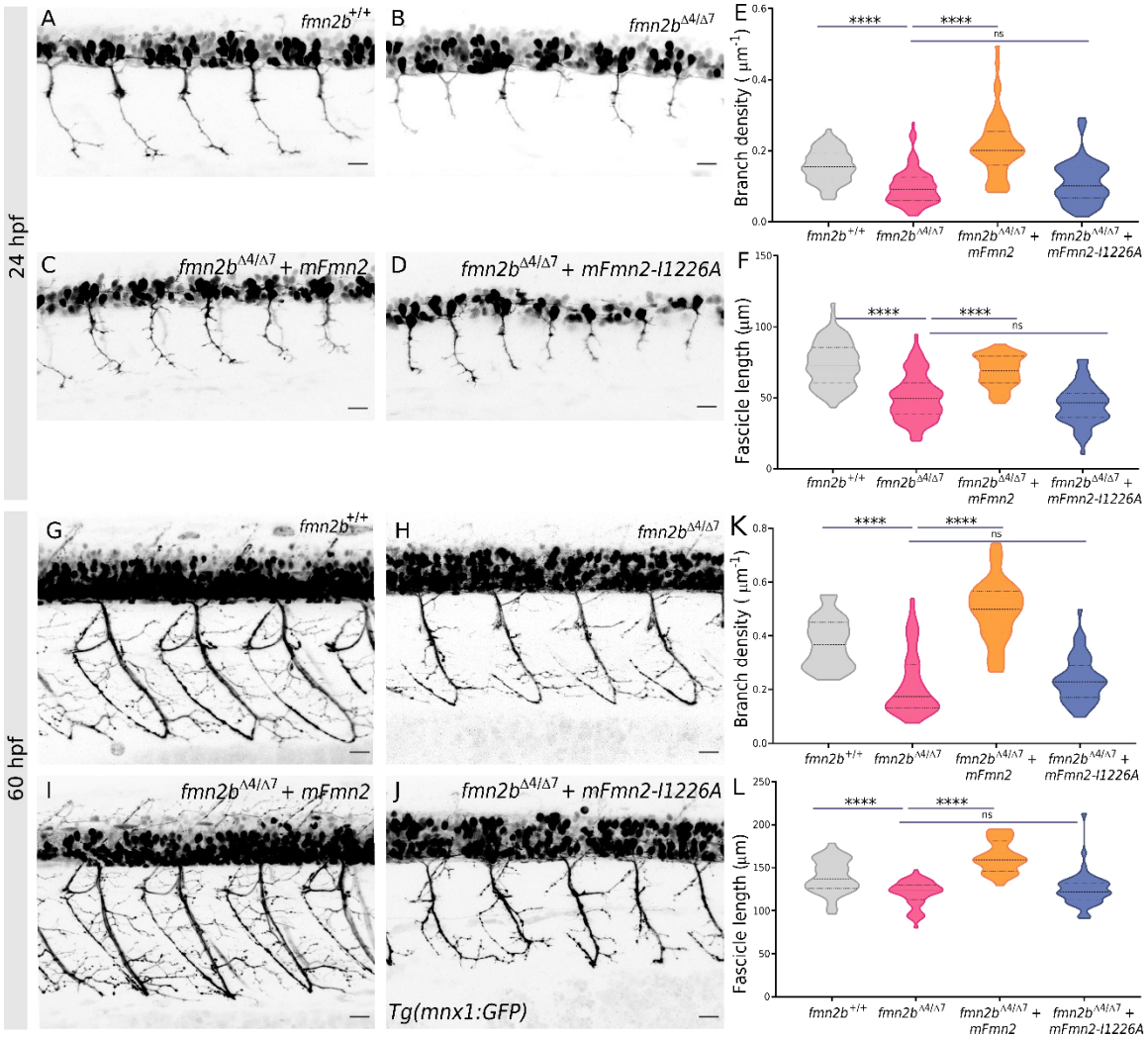

Figure 4. Motor neuron outgrowth and branching defects in *fmn2b* mutants

Representative micrographs of motor neurons labelled by *Tg(mnx1:GFP)* in 24 hpf **A)** *fmn2b*$^{+/+}$ and **B)** *fmn2b*$^{\Delta4/\Delta7}$ and 60 hpf **G)** *fmn2b*$^{+/+}$ and **H)** *fmn2b*$^{\Delta4/\Delta7}$ embryos. Motor neurons visualized by *Tg(mnx1:GFP)* in *fmn2b*$^{\Delta4/\Delta7}$ mutant embryos injected at 1-cell stage with full-length mouse Fmn2 (mFmn2) mRNA at **C)** 24 hpf and **I)** 60 hpf and nucleation dead mouse Fmn2 (mFmn2-I1226A) mRNA at **D)** 24 hpf and **J)** 60 hpf. **E)** Quantification of branch density (number of branches per fascicle normalized to the fascicle length) per myotome hemisegment in 24 hpf *fmn2b*$^{+/+}$ (0.1571 ± 0.005 µm^{-1}; n=70 hemisegments) and *fmn2b*$^{\Delta4/\Delta7}$ embryos (0.0981 ± 0.005 µm^{-1}; n=118 hemisegments). The defects were rescued in *fmn2b*$^{\Delta4/\Delta7}$ embryos injected with

mFmn2 mRNA (0.2139 ± 0.012 μm^{-1}; n=51 hemisegments) but not in the embryos injected with mFmn2-I1226A mRNA (0.111 ± 0.007 μm^{-1}; n=63 hemisegments). **F)** Quantification of fascicle length extended by motor neurons per myotome hemisegment in 24 hpf *fmn2b*$^{+/+}$ (68.97 ± 1.55 µm; n=70 hemisegments) and *fmn2b*$^{\Delta 4/\Delta 7}$ embryos (44.98 ± 1.756 µm; n=118 hemisegments). The defects were rescued in *fmn2b*$^{\Delta 4/\Delta 7}$ embryos injected with mFmn2 mRNA (73.7 ± 1.86 µm; n=51 hemisegments) but not in the embryos injected with mFmn2-I1226A mRNA (73.7 ± 1.86 µm; n=63 hemisegments). **K)** Quantification of branch density (number of branches per fascicle normalized to the fascicle length) per myotome hemisegment in 60 hpf *fmn2b*$^{+/+}$ (0.3746 ± 0.014 μm^{-1}; n=37 hemisegments) and *fmn2b*$^{\Delta 4/\Delta 7}$ embryos (0.2211 ± 0.015 μm^{-1}; n=57 hemisegments). The defects were rescued in *fmn2b*$^{\Delta 4/\Delta 7}$ embryos injected with mFmn2 mRNA (0.4955 ± 0.021 μm^{-1}; n=30 hemisegments) but not in the embryos injected with mFmn2-I1226A mRNA (0.2369 ± 0.012 μm^{-1}; n=48 hemisegments). **L)** Quantification of fascicle length extended by motor neurons per myotome hemisegment in 60 hpf *fmn2b*$^{+/+}$ (139.6 ± 3.21 µm; n=37 hemisegments) and *fmn2b*$^{\Delta 4/\Delta 7}$ embryos (120.4 ± 1.94 µm; n=57 hemisegments). The defects were rescued in *fmn2b*$^{\Delta 4/\Delta 7}$ embryos injected with mFmn2 mRNA (162.7 ± 3.38 µm; n=30 hemisegments) but not in the embryos injected with mFmn2-I1226A mRNA (124.7 ± 2.81 µm; n=48 hemisegments). (**** p-value <0.0001; ns - not significant; Kruskal Wallis test followed by Dunn's post-hoc analysis). Scale bar is equivalent to 20 µm.

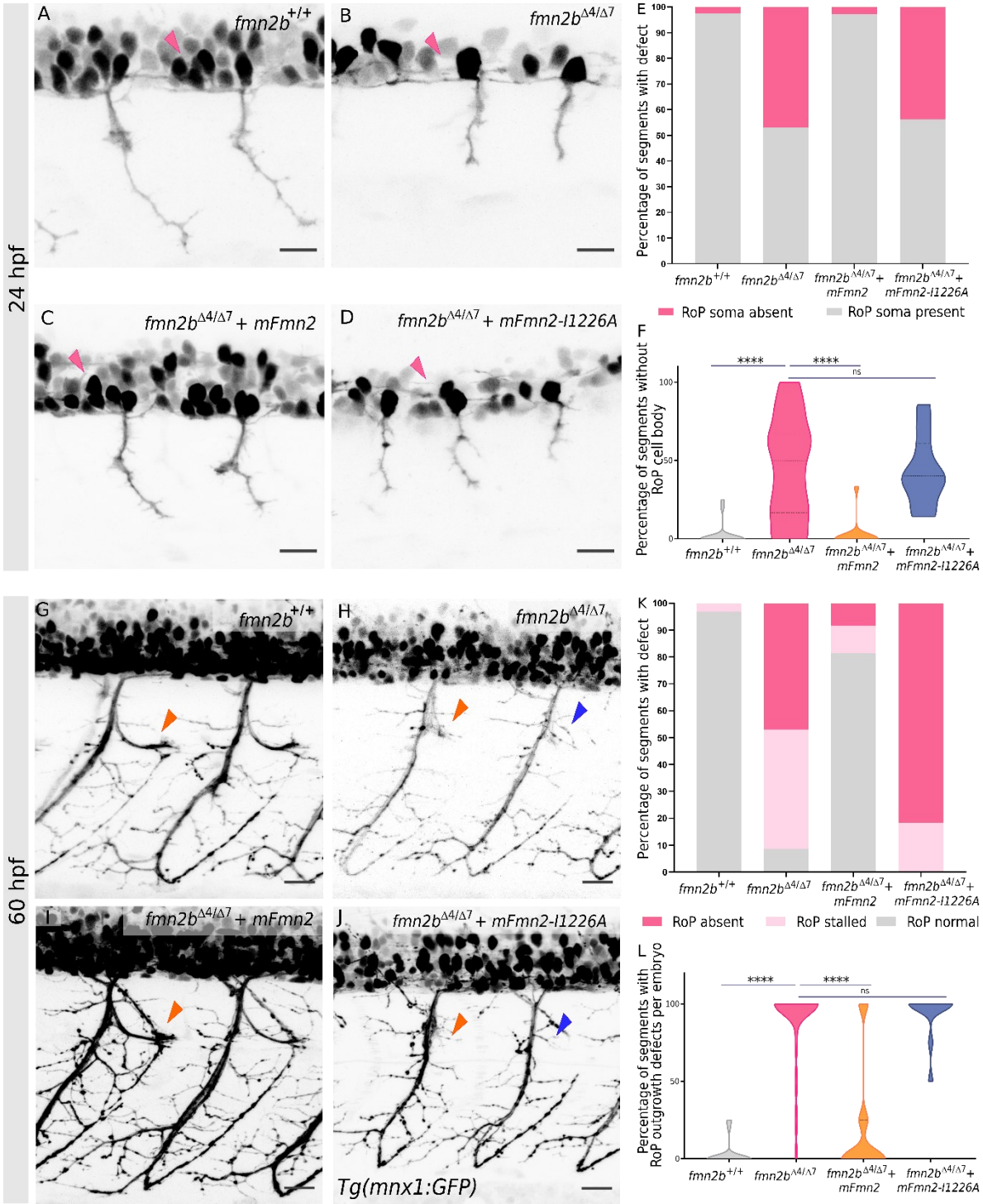

661

662 **Figure 5. RoP soma and lateral innervation of the myotome by RoP are affected**

663 **in *fmn2b* mutants**

664 Representative micrographs of motor neurons labelled by *Tg(mnx1:GFP)* in 24 hpf **A)**

665 *fmn2b*$^{+/+}$ and **B)** *fmn2b*$^{\Delta4/\Delta7}$ embryos. Representative micrographs of motor neurons

666 labelled by *Tg(mnx1:GFP)* in 24 hpf old *fmn2b*$^{\Delta4/\Delta7}$ mutant embryos injected at 1-cell

667 stage with **C)** full-length mouse Fmn2 (mFmn2) mRNA and **D)** nucleation dead
668 version, mFmn2-I1226A mRNA. The pink arrowheads indicate the RoP soma or its
669 expected position. **E)** Bar graph summarizing the percentage of embryos with defects
670 in RoP soma in 24 hpf *fmn2b*$^{+/+}$ (n=18) and *fmn2b*$^{\Delta4/\Delta7}$ embryos (n=23). The defects
671 were rescued in *fmn2b*$^{\Delta4/\Delta7}$ embryos injected with mFmn2 mRNA (n=12) but not in the
672 embryos injected with mFmn2-I1226A mRNA (n=10*).* $\chi2$ test of independence shows
673 significant difference between the four groups, $\chi2$ (df = 3) =101.8 , $p < 0.0001$. **F)** Violin
674 plots depicting the variation in data summarized in the bar graphs for 24 hpf embryos.
675 (**** p-value <0.0001; ns - not significant; Kruskal Wallis test followed by Dunn's post-
676 hoc analysis). Scale bar is equivalent to 20 μm.

677 Representative micrographs of motor neurons labelled by *Tg(mnx1:GFP)* in 60 hpf **G)**
678 *fmn2b*$^{+/+}$ and **H)** *fmn2b*$^{\Delta4/\Delta7}$ embryos. Representative micrographs of motor neurons
679 labelled by *Tg(mnx1:GFP)* in 60 hpf old *fmn2b*$^{\Delta4/\Delta7}$ mutant embryos injected at 1-cell
680 stage with **I)** full-length mouse Fmn2 (mFmn2) mRNA and **J)** nucleation dead version,
681 mFmn2-I1226A mRNA. The orange arrowheads point towards the stalled RoP and the
682 blue arrowheads indicate no RoP outgrowth. **K)** Bar graphs summarizing the
683 percentage of embryos with defects in RoP axon outgrowth in 60 hpf *fmn2b*$^{+/+}$ (n=22)
684 and *fmn2b*$^{\Delta4/\Delta7}$ embryos (n=26). The defects were rescued in *fmn2b*$^{\Delta4/\Delta7}$ embryos
685 injected with mFmn2 mRNA (n=14) but not in the embryos injected with mFmn2-
686 I1226A mRNA (n=13). $\chi2$ test of independence shows significant difference between
687 the four groups, $\chi2$ (df = 6) = 332.7, $p < 0.0001$. **L)** Violin plots depicting the variation
688 in data summarized in the bar graphs for 60 hpf embryos. (**** p-value <0.0001; ns -
689 not significant; Kruskal Wallis test followed by Dunn's post-hoc analysis) Scale bar is
690 equivalent to 20 μm.

691

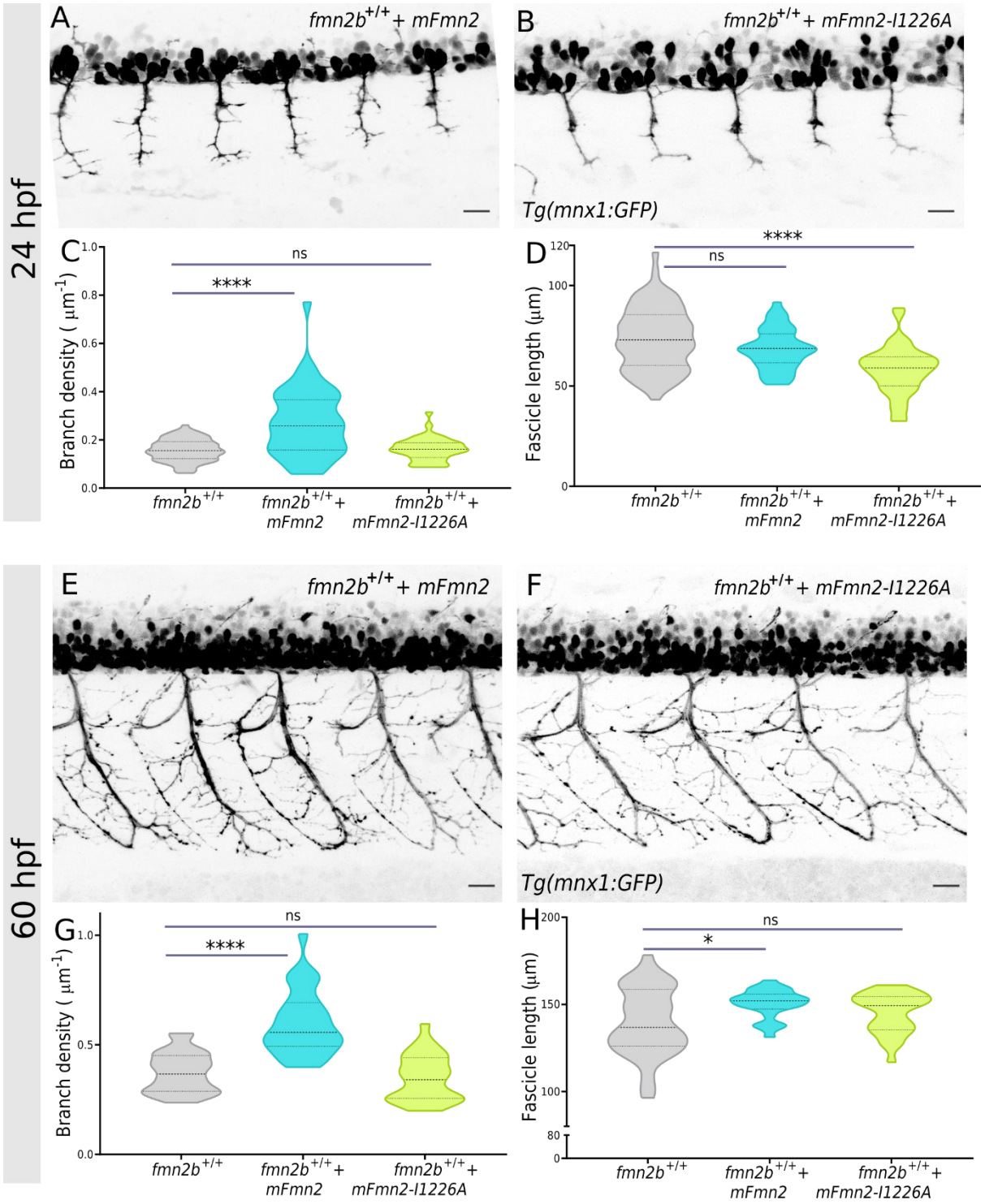

692

693 **Figure 6. Outgrowth and branching phenotypes upon overexpression of mouse**

694 **Fmn2 in wild-type embryos**

695 Representative micrographs of motor neurons labelled by *Tg(mnx1:GFP)* in 24 hpf old

696 *fmn2b*$^{+/+}$ embryos injected with **A)** mFmn2 mRNA and **B)** mFmn2-I1226A mRNA. **C)**

697 Quantification of branch density (number of branches per fascicle normalized to the
698 fascicle length) along the fascicle extended by motor neurons per myotome
699 hemisegment in *fmn2b*$^{+/+}$ embryos injected with mFmn2 mRNA (0.2728 ± 0.0217 μm^{-1};
700 n=40 hemisegments) and mFmn2-I1226A mRNA (0.1617 ± 0.007 μm^{-1}; n=40
701 hemisegments). **D)** Quantification of fascicle length extended by motor neurons per
702 myotome hemisegment in *fmn2b*$^{+/+}$ embryos injected with mFmn2 mRNA (73.7 ± 1.86
703 µm; n=40 hemisegments) and mFmn2-I1226A mRNA (68.3 ± 1.603 µm; n=40
704 hemisegments). Representative micrographs of motor neurons labelled by
705 *Tg(mnx1:GFP)* in 60 hpf old *fmn2b*$^{+/+}$ embryos injected with **E)** mFmn2 mRNA and **F)**
706 mFmn2-I1226A mRNA. **G)** Quantification of branch density (number of branches per
707 fascicle normalized to the fascicle length) along the fascicle extended by motor
708 neurons per myotome hemisegment in 60 hpf *fmn2b*$^{+/+}$ embryos injected with mFmn2
709 mRNA (0.599 ± 0.027 μm^{-1}; n=28 hemisegments) and mFmn2-I1226A mRNA (0.3481
710 ± 0.02 μm^{-1}; n=28 hemisegments). **H)** Quantification of fascicle length extended by
711 motor neurons per myotome hemisegment in 60 hpf *fmn2b*$^{+/+}$ embryos injected with
712 mFmn2 mRNA (150.4 ± 1.536 µm; n=28 hemisegments) and mFmn2-I1226A mRNA
713 (145 ± 2.18 µm; n=28 hemisegments). (**** p-value <0.0001; * p-value = 0.0175; ns -
714 not significant; Kruskal Wallis test followed by Dunn's post-hoc analysis) Scale bar is
715 equivalent to 20 µm.

716

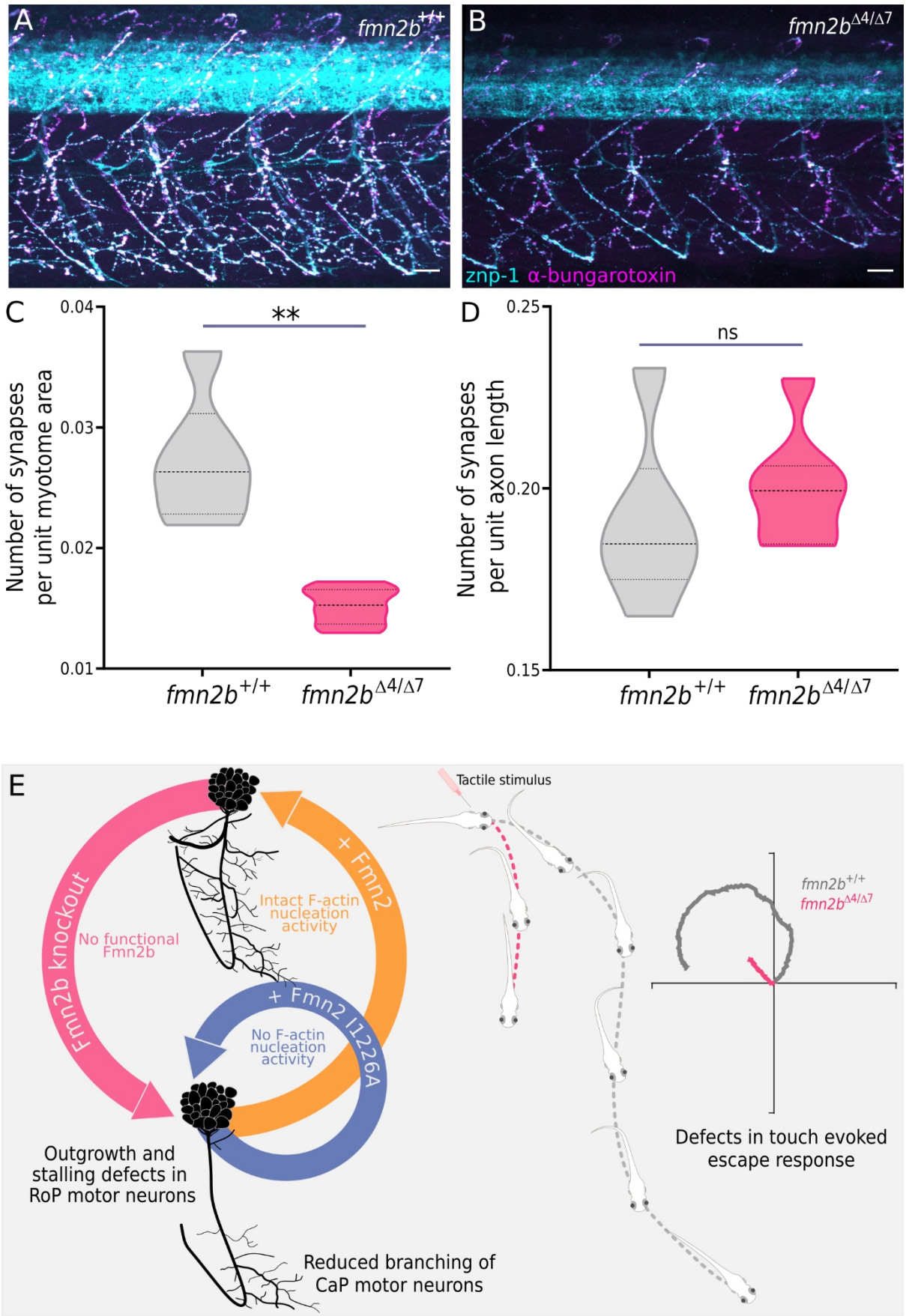

717

718 **Figure 7. Synapse coverage in *fmn2b* mutants**

719 Representative micrographs of 60 hpf **A)** *fmn2b*$^{+/+}$ (n=6) **B)** *fmn2b*$^{\Delta 4/\Delta 7}$ embryos (n=7)
720 co-stained with znp-1 antibody and α-bungarotoxin. Quantification of colocalization of
721 znp-1 and α-bungarotoxin in NMJ structures of 60 hpf embryos. **C)** Number of
722 synapses per unit myotome area in *fmn2b*$^{+/+}$ (0.0272 ±0.002; n=6) and *fmn2b*$^{\Delta 4/\Delta 7}$
723 embryos (0.01521 ±0.0005; n=7, **p-value=0.0012). **D)** Number of synapses per unit
724 axon length in *fmn2b*$^{+/+}$ (0.1903± 0.009; n=6) and *fmn2b*$^{\Delta 4/\Delta 7}$ embryos (0.2001± 0.005;
725 n=7). (ns- not significant; Mann Whitney U test) Scale bar is equivalent to 20 μm. **E)**
726 Depletion of Fmn2b causes outgrowth and branching defects in motor neurons in
727 zebrafish larvae causing defects in motor behaviours. The outgrowth and branching
728 defects in *fmn2b* mutants can be rescued by expression of full-length mouse Fmn2 in
729 the mutants highlighting the requirement and conserved function of Fmn2 in
730 development of motor neurons *in vivo*. The inability of mFmn2-I1226A to rescue the
731 defects in *fmn2b* mutants underscores the requirement of the F-actin nucleation
732 activity of Fmn2 in outgrowth and branching of motor neurons. The blue and orange
733 curved arrows indicate the rescue experiments with full length mFmn2 and nucleation
734 dead mFmn2-I1226A in the *fmn2b* mutant background respectively. The grey and pink
735 traces indicate the trajectories of wildtype and *fmn2b* mutant embryos respectively in
736 response to tactile stimulus. The schematic is not drawn to scale.

REFERENCES

Agís-Balboa RC et al. (2017) Formin 2 links neuropsychiatric phenotypes at young age to an increased risk for dementia. EMBO J 36:2815–2828.

Ahuja R, Pinyol R, Reichenbach N, Custer L, Klingensmith J, Kessels MM, Qualmann B (2007) Cordon-Bleu Is an Actin Nucleation Factor and Controls Neuronal Morphology. Cell 131:337–350.

Armijo-Weingart L, Gallo G (2017) It takes a village to raise a branch: Cellular mechanisms of the initiation of axon collateral branches. Mol Cell Neurosci 84:36–47.

Atkins M, Gasmi L, Bercier V, Revenu C, Del Bene F, Hazan J, Fassier C (2019) FIGNL1 associates with KIF1Bβ and BICD1 to restrict dynein transport velocity during axon navigation. J Cell Biol 218:3290–3306.

Bagnall MW, McLean DL (2014) Modular Organization of Axial Microcircuits in Zebrafish. Science (80-) 343:197–200.

Balasanyan V, Watanabe K, Dempsey WP, Lewis TL, Trinh LA, Arnold DB (2017) Structure and Function of an Actin-Based Filter in the Proximal Axon. Cell Rep 21:2696–2705.

Beattie CE, Hatta K, Halpern ME, Liu H, Eisen JS, Kimmel CB (1997) Temporal separation in the specification of primary and secondary motoneurons in zebrafish. Dev Biol 187:171–182.

Bello-Rojas S, Istrate AE, Kishore S, McLean DL (2019) Central and peripheral innervation patterns of defined axial motor units in larval zebrafish. J Comp Neurol 527:2557–2572.

760 Bernhardt RR, Chitnis AB, Lindamer L, Kuwada JY (1990) Identification of spinal
761 neurons in the embryonic and larval zebrafish. J Comp Neurol 302:603–616.

762 Bresciani E, Broadbridge E, Liu PP (2018) An efficient dissociation protocol for
763 generation of single cell suspension from zebrafish embryos and larvae.
764 MethodsX 5:1287–1290.

765 Brustein E, Saint-Amant L, Buss RR, Chong M, McDearmid JR, Drapeau P (2003)
766 Steps during the development of the zebrafish locomotor network. J Physiol Paris
767 97:77–86.

768 Carrington B, Varshney GK, Burgess SM, Sood R (2015) CRISPR-STAT: An easy and
769 reliable PCR-based method to evaluate target-specific sgRNA activity. Nucleic
770 Acids Res 43:e157.

771 Chia PH, Chen B, Li P, Rosen MK, Shen K (2014) Local F-actin network links synapse
772 formation and axon branching. Cell 156:208–220.

773 Coles CH, Bradke F (2015) Coordinating Neuronal Actin-Microtubule Dynamics. Curr
774 Biol 25:R677–R691.

775 Colombo A, Palma K, Armijo L, Mione M, Signore IA, Morales C, Guerrero N, Meynard
776 MM, Pérez R, Suazo J, Marcelain K, Briones L, Härtel S, Wilson SW, Concha ML
777 (2013) Daam1a mediates asymmetric habenular morphogenesis by regulating
778 dendritic and axonal outgrowth. Dev 140:3997–4007.

779 Das R, Bhattacharjee S, Letcher JM, Harris JM, Nanda S, Foldi I, Lottes EN, Bobo
780 HM, Grantier BD, Mihály J, Ascoli GA, Cox DN (2021) Formin3 directs dendritic
781 architecture via microtubule regulation and is required for somatosensory
782 nociceptive behavior. Development.

783 Dent EW, Gupton SL, Gertler FB (2011) The growth cone cytoskeleton in Axon

784 outgrowth and guidance. Cold Spring Harb Perspect Biol 3:1–39.

785 Dickson BJ (2002) Molecular mechanisms of axon guidance. Science (80-) 298:1959–
786 1964.

787 Drapeau P, Saint-Amant L, Buss RR, Chong M, McDearmid JR, Brustein E (2002)
788 Development of the locomotor network in zebrafish. Prog Neurobiol 68:85–111.

789 Eisen JS, Myers PZ, Westerfield M (1986) Pathway selection by growth cones of
790 identified motoneurones in live zebra fish embryos. Nature 320:269–271.

791 Fassier C, Fréal A, Gasmi L, Delphin C, Ten Martin D, De Gois S, Tambalo M, Bosc
792 C, Mailly P, Revenu C, Peris L, Bolte S, Schneider-Maunoury S, Houart C,
793 Nothias F, Larcher J-C, Andrieux A, Hazan J (2018) Motor axon navigation relies
794 on Fidgetin-like 1-driven microtubule plus end dynamics. J Cell Biol 217:1719–
795 1738.

796 Flanagan-Steet H, Fox MA, Meyer D, Sanes JR (2005) Neuromuscular synapses can
797 form in vivo by incorporation of initially aneural postsynaptic specializations.
798 Development 132:4471–4481.

799 Flynn KC, Bradke F (2020) Role of the cytoskeleton and membrane trafficking in axon–
800 dendrite morphogenesis. In: Cellular Migration and Formation of Axons and
801 Dendrites, pp 21–56. Elsevier.

802 Gallo G (2011) The cytoskeletal and signaling mechanisms of axon collateral
803 branching. Dev Neurobiol 71:201–220.

804 Gallo G (2016) Coordination of the axonal cytoskeleton during the emergence of axon
805 collateral branches. Neural Regen Res 11:709–711.

806 Ghate K, Mutalik SP, Sthanam LK, Sen S, Ghose A (2020) Fmn2 Regulates Growth

807 Cone Motility by Mediating a Molecular Clutch to Generate Traction Forces.
808 Neuroscience 448:160–171.

809 González-Fraga J, Dipp-Alvarez V, Bardullas U (2019) Quantification of Spontaneous
810 Tail Movement in Zebrafish Embryos Using a Novel Open-Source MATLAB
811 Application. Zebrafish 16:214–216.

812 Goode BL, Eck MJ (2007) Mechanism and Function of Formins in the Control of Actin
813 Assembly. Annu Rev Biochem 76:593–627.

814 Gordon-Weeks PR, Fournier AE (2014) Neuronal cytoskeleton in synaptic plasticity
815 and regeneration. J Neurochem 129:206–212.

816 Gorukmez O, Gorukmez O, Ekici A (2020) A Novel Nonsense FMN2 Mutation in
817 Nonsyndromic Autosomal Recessive Intellectual Disability Syndrome. Fetal
818 Pediatr Pathol.

819 Hale ME, Ritter D a., Fetcho JR (2001) A confocal study of spinal interneurons in living
820 larval zebrafish. J Comp Neurol 437:1–16.

821 Hu J, Bai X, Bowen JR, Dolat L, Korobova F, Yu W, Baas PW, Svitkina T, Gallo G,
822 Spiliotis ET (2012) Septin-driven coordination of actin and microtubule remodeling
823 regulates the collateral branching of axons. Curr Biol 22:1109–1115.

824 Kessels MM, Schwintzer L, Schlobinski D, Qualmann B (2011) Controlling actin
825 cytoskeletal organization and dynamics during neuronal morphogenesis. Eur J
826 Cell Biol 90:926–933.

827 Ketschek A, Gallo G (2010) Nerve Growth Factor Induces Axonal Filopodia through
828 Localized Microdomains of Phosphoinositide 3-Kinase Activity That Drive the
829 Formation of Cytoskeletal Precursors to Filopodia. J Neurosci 30:12185–12197.

Ketschek A, Jones S, Spillane M, Korobova F, Svitkina T, Gallo G (2015) Nerve growth factor promotes reorganization of the axonal microtubule array at sites of axon collateral branching. Dev Neurobiol 75:1441–1461.

Ketschek A, Spillane M, Dun XP, Hardy H, Chilton J, Gallo G (2016) Drebrin coordinates the actin and microtubule cytoskeleton during the initiation of axon collateral branches. Dev Neurobiol 76:1092–1110.

Kimmel CB, Ballard WW, Kimmel SR, Ullmann B, Schilling TF (1995) Stages of embryonic development of the zebrafish. Dev Dyn 203:253–310.

Kundu T, Das SS, Kumar DS, Sewatkar LK, Ghose A (2020) Antagonistic activities of Fmn2 and ADF regulate axonal F-actin patch dynamics and the initiation of collateral branching. bioRxiv:2020.11.16.384099.

Kundu T, Dutta P, Nagar D, Maiti S, Ghose A (2021) Coupling of dynamic microtubules to F-actin by Fmn2 regulates chemotaxis of neuronal growth cones. J Cell Sci.

Kuwada JY (1993) Pathway selection by growth cones in the zebrafish central nervous system. Perspect Dev Neurobiol 1:195–203.

LaFave MC, Varshney GK, Vemulapalli M, Mullikin JC, Burgess SM (2014) A Defined Zebrafish Line for High-Throughput Genetics and Genomics: NHGRI-1. Genetics 198:167–170.

Langebeck-Jensen K, Shahar OD, Schuman EM, Langer JD, Ryu S (2019) Larval Zebrafish Proteome Regulation in Response to an Environmental Challenge. Proteomics 19:1900028.

Law R et al. (2014) Biallelic truncating mutations in FMN2, encoding the actin-regulatory protein formin 2, cause nonsyndromic autosomal-recessive intellectual disability. Am J Hum Genet 95:721–728.

854 Leader B, Leder P (2000) Formin-2, a novel formin homology protein of the cappuccino
855 subfamily, is highly expressed in the developing and adult central nervous system.

856 Lewis TL, Courchet J, Polleux F (2013) Cellular and molecular mechanisms underlying
857 axon formation, growth, and branching. J Cell Biol 202:837–848.

858 Lian G, Dettenhofer M, Lu J, Downing M, Chenn A, Wong T, Sheen V (2016) Filamin
859 A- and formin 2-dependent endocytosis regulates proliferation via the canonical
860 wnt pathway. Dev 143:4509–4520.

861 Liu LYM, Lin MH, Lai ZY, Jiang JP, Huang YC, Jao LE, Chuang YJ (2016) Motor
862 neuron-derived Thsd7a is essential for zebrafish vascular development via the
863 Notch-dll4 signaling pathway. J Biomed Sci 23:1–11.

864 Lowery LA, Van Vactor D (2009) The trip of the tip: understanding the growth cone
865 machinery. Nat Rev Mol Cell Biol 10:332–343.

866 Marco EJ, Aitken AB, Nair VP, da Gente G, Gerdes MR, Bologlu L, Thomas S, Sherr
867 EH (2018) Burden of de novo mutations and inherited rare single nucleotide
868 variants in children with sensory processing dysfunction. BMC Med Genomics
869 11:50.

870 Matusek T, Gombos R, Szécsényi A, Sánchez-Soriano N, Czibula Á, Pataki C, Gedai
871 A, Prokop A, Raskó I, Mihály J (2008) Formin Proteins of the DAAM Subfamily
872 Play a Role during Axon Growth. J Neurosci 28:13310 LP – 13319.

873 McLean DL, Fetcho JR (2008) Using imaging and genetics in zebrafish to study
874 developing spinal circuits in vivo. Dev Neurobiol 68:817–834.

875 Melançon E, Liu DWC, Westerfield M, Eisen JS (1997) Pathfinding by identified
876 zebrafish motoneurons in the absence of muscle pioneers. J Neurosci 17:7796–
877 7804.

878 Menelaou E, Svoboda KR (2009) Secondary motoneurons in juvenile and adult
879 zebrafish: Axonal pathfinding errors caused by embryonic nicotine exposure. J
880 Comp Neurol 512:305–322.

881 Menon S, Gupton S (2018) Recent advances in branching mechanisms underlying
882 neuronal morphogenesis .

883 Montaville P, Jégou A, Pernier J, Compper C, Guichard B, Mogessie B, Schuh M,
884 Romet-Lemonne G, Carlier MF (2014) Spire and Formin 2 Synergize and
885 Antagonize in Regulating Actin Assembly in Meiosis by a Ping-Pong Mechanism.
886 PLoS Biol 12.

887 Montaville P, Kühn S, Compper C, Carlier MF (2016) Role of the C-terminal extension
888 of formin 2 in its activation by spire protein and processive assembly of actin
889 filaments. J Biol Chem 291:3302–3318.

890 Morello G, Guarnaccia M, Spampinato AG, La Cognata V, D'Agata V, Cavallaro S
891 (2018) Copy Number Variations in Amyotrophic Lateral Sclerosis: Piecing the
892 Mosaic Tiles Together through a Systems Biology Approach. Mol Neurobiol
893 55:1299–1322.

894 Moreno-Mateos MA, Vejnar CE, Beaudoin J-D, Fernandez JP, Mis EK, Khokha MK,
895 Giraldez AJ (2015) CRISPRscan: designing highly efficient sgRNAs for CRISPR-
896 Cas9 targeting in vivo. Nat Methods 2015 1210 12:982–988.

897 Myers PZ, Eisen JS, Westerfield M (1986) Development and Axonal Outgrowth of
898 Identified Motoneurons in the Zebrafish.

899 Nagar D, James TK, Mishra R, Guha S, Burgess SM, Ghose A (2021) The Formin
900 Fmn2b Is Required for the Development of an Excitatory Interneuron Module in
901 the Zebrafish Acoustic Startle Circuit. eNeuro 8:ENEURO.0329-20.2021.

902 Nithianandam V, Chien C-T (2018) Actin blobs prefigure dendrite branching sites. J
903 Cell Biol 217:3731–3746.

904 Pamphlett R, Morahan JM, Luquin N, Yu B (2011) Looking for differences in copy
905 number between blood and brain in sporadic amyotrophic lateral sclerosis.
906 Muscle Nerve 44:492–498.

907 Perrone MD, Rocca MS, Bruno I, Faletra F, Pecile V, Gasparini P (2012) De novo 911
908 Kb interstitial deletion on chromosome 1q43 in a boy with mental retardation and
909 short stature. Eur J Med Genet 55:117–119.

910 Pike SH, Melancon EF, Eisen JS (1992) Pathfinding by zebrafish motoneurons in the
911 absence of normal pioneer axons. Development 114:825–831.

912 Prokop A, Sánchez-Soriano N, Gonçalves-Pimentel C, Molnár I, Kalmár T, Mihály J
913 (2011) DAAM family members leading a novel path into formin research. Commun
914 Integr Biol 4:538–542.

915 Quinlan ME, Hilgert S, Bedrossian A, Mullins RD, Kerkhoff E (2007) Regulatory
916 interactions between two actin nucleators, Spire and Cappuccino. J Cell Biol
917 179:117–128.

918 Roth-Johnson EA, Vizcarra CL, Bois JS, Quinlan ME (2014) Interaction between
919 microtubules and the drosophila formin cappuccino and its effect on actin
920 assembly. J Biol Chem 289:4395–4404.

921 Sahasrabudhe A, Ghate K, Mutalik S, Jacob A, Ghose A (2016) Formin 2 regulates
922 the stabilization of filopodial tip adhesions in growth cones and affects neuronal
923 outgrowth and pathfinding in vivo. Dev 143:449–460.

924 Saint-Amant L, Drapeau P (1998) Time course of the development of motor behaviors
925 in the zebrafish embryo. J Neurobiol 37:622–632.

926 Schymick JC, Scholz SW, Fung H-C, Britton A, Arepalli S, Gibbs JR, Lombardo F,
927 Matarin M, Kasperaviciute D, Hernandez DG, Crews C, Bruijn L, Rothstein J,
928 Mora G, Restagno G, Chiò A, Singleton A, Hardy J, Traynor BJ (2007) Genome-
929 wide genotyping in amyotrophic lateral sclerosis and neurologically normal
930 controls: first stage analysis and public release of data. Lancet Neurol 6:322–328.

931 Spillane M, Gallo G (2014) Involvement of Rho-family GTPases in axon branching.
932 Small GTPases 5.

933 Spillane M, Ketschek A, Jones SL, Korobova F, Marsick B, Lanier L, Svitkina T, Gallo
934 G (2011) The actin nucleating Arp2/3 complex contributes to the formation of
935 axonal filopodia and branches through the regulation of actin patch precursors to
936 filopodia. Dev Neurobiol 71:747–758.

937 Stifani N (2014) Motor neurons and the generation of spinal motor neuron diversity.
938 Front Cell Neurosci 8:293.

939 Varshney GK, Carrington B, Pei W, Bishop K, Chen Z, Fan C, Xu L, Jones M, LaFave
940 MC, Ledin J, Sood R, Burgess SM (2016) A high-throughput functional genomics
941 workflow based on CRISPR/Cas9-mediated targeted mutagenesis in zebrafish.
942 Nat Protoc 11:2357–2375.

943 Varshney GK, Pei W, Lafave MC, Idol J, Xu L, Gallardo V, Carrington B, Bishop K,
944 Jones M, Li M, Harper U, Huang SC, Prakash A, Chen W, Sood R, Ledin J,
945 Burgess SM (2015) High-throughput gene targeting and phenotyping in zebrafish
946 using CRISPR/Cas9. Genome Res 25:1030–1042.

947 Westerfield M, McMurray J V., Eisen JS (1986) Identified motoneurons and their
948 innervation of axial muscles in the zebrafish. J Neurosci 6:2267–2277.

949 Yoo H, Roth-Johnson EA, Bor B, Quinlan ME (2015) Drosophila Cappuccino alleles

provide insight into formin mechanism and role in oogenesis. Mol Biol Cell 26:1875–1886.

ACKNOWLEDGEMENTS

The authors thank Dr. N. K. Subhedar (IISER Pune) for critical inputs on the manuscript. The authors acknowledge the IISER Pune Microscopy Facility, the National Facility for Gene Function in Health and Disease (NFGFHD) at IISER Pune and the zebrafish facility at NHGRI Zebrafish Core, NIH for access to equipment and infrastructure.

FUNDING

The study was supported from grants from the Council of Scientific and Industrial Research, Govt of India (37(1689)/17/EMR-II), Department of Biotechnology, Govt. of India (BT/PR26241/GET/119/244/2017) and intramural support from IISER Pune to A.G.. D.N. is supported by a fellowship from the Council of Scientific and Industrial Research, Govt of India. D.N. was awarded the Indo-U.S. GETin Internship (2018_050) (Department of Biotechnology (DBT), Government of India and Indo US Science and Technology Forum (IUSSTF)) which supported the CRISPR Cas9 mutagenesis work at NHGRI, NIH. The National Facility for Gene Function in Health and Disease (NFGFHD) at IISER Pune is supported by the Department of Biotechnology, Govt. of India (BT/INF/22/SP17358/2016). S.M.B. is supported by the Intramural Research Program of the National Human Genome Research Institute (ZIAHG200386-06).

AUTHOR INFORMATION

AFFILIATIONS

1. **Indian Institute of Science Education and Research (IISER) Pune, Dr Homi Bhabha Road, Pune 411008, INDIA**

   Dhriti Nagar and Aurnab Ghose

2. **Zebrafish Core, Translational and Functional Genomics Branch, National Human Genome Research Institute, National Institutes of Health, Bethesda, Maryland, USA**

   Blake Carrington

3. **Translational and Functional Genomics Branch, National Human Genome Research Institute (NHGRI), National Institutes of Health (NIH), Bethesda, MD, USA**

   Shawn M Burgess

CONTRIBUTION

Conceptualization: D.N. and A.G.; Investigation and formal analysis: D.N.; Methodology and resources: B.C. and S.M.B.; Writing – original draft: D.N. and A.G.; Writing – review and editing: D.N., B.C., S.M.B. and A.G; Funding Acquisition: A.G.. All authors gave final approval for publication and agreed to be held accountable for the work performed therein.

CORRESPONDING AUTHORS

Correspondence: Dr. Aurnab Ghose, Indian Institute of Science Education and Research (IISER) Pune, Dr Homi Bhabha Road, Pune 411008, INDIA.

Email: aurnab@iiserpune.ac.in

ETHICS DECLARATIONS

Ethics approval

All zebrafish husbandry and experimental protocols complied with institutional guidelines and were approved by the Institute Animal Ethics Committee (IAEC) and the Institutional Biosafety Committee (IBSC), IISER Pune or a National Human Genome Research Institute (NHGRI/NIH) Animal Care and Use Committee approved animal study protocol.

Consent for publication

All authors gave consent for publication.

Competing interests

The authors declare no competing interests.